ELSEVIER

Volume 182, Number 12, December 2009

JOURNAL OF SOLID STATE CHEMISTRY

www.elsevier.com/locate/jssc

CONTENTS

Abstracted/indexed in BioEngineering Abstracts, Chemical Abstracts, Coal Abstracts, Current Contents/Physics, Chemical, & Earth Sciences, Engineering Index, Research Alert, SCISEARCH, Science Abstracts, and Science Citation Index. Also covered in the abstract and citation database SCOPUS®. Full text available on ScienceDirect®.

Regular Articles

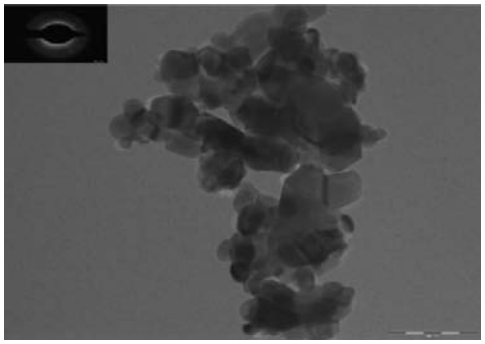

The synthesized nanoparticles shapes, sizes and size dispersibilities were obtained from the transmission electron microscopy (TEM). The TEM micrographs of synthesized samples revealed that, spherical shape with average particle size 50 nm. Selected area electron diffraction pattern (SAED) suggests the polycrystallinity and also the formation of spinel ferrites.

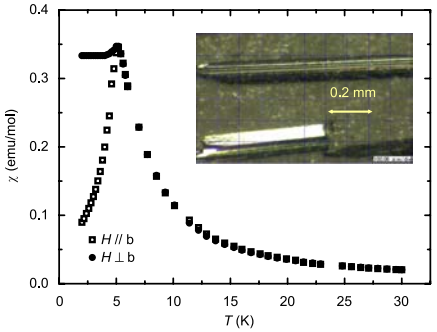

The temperature dependence of the magnetic susceptibility of V_3O_7 for ($H \| b$) and ($H \perp b$), respectively, at 0.1 T. The inset shows crystals of V_3O_7 grown by using NH_4Cl as the transport agent.

Regular Articles—Continued

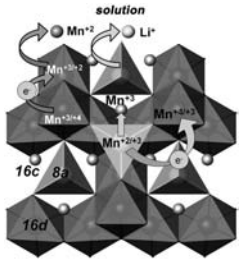

Schematic representation of the acid leaching of $LiMn_{2-y}Ti_yO_4$ ($0.2 \le y \le 1.0$).

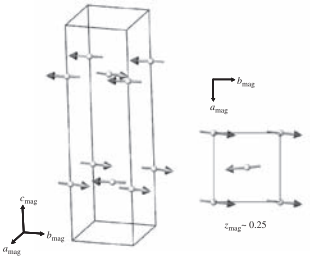

The metal telluromolybdates $Co_{1-x}Zn_xTeMoO_6$ have an orthorhombic structure with space group $P2_12_12$. In this structure, M ions form a pseudo-square-planer lattice in the *ab* plane. These compounds show a low-dimensional magnetism reflecting this structural feature. The magnetic transition observed in the $CoTeMoO_6$ is a canted antiferromagnetic ordering of Co^{2+} ions, and the figure is the magnetic structure.

Continued

Preparation and characterization of Zr doped TiO_2 nanotube arrays on the titanium sheet and their enhanced photocatalytic activity
Haijin Liu, Guoguang Liu and Qingxiang Zhou
Page 3238

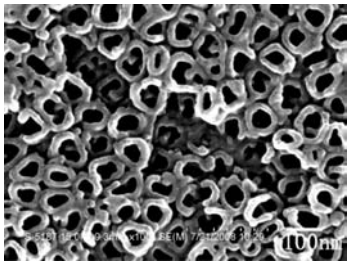

Zr-doped TiO_2 nanotube arrays were prepared by two-step electrochemical process. The photocatalytic efficiency of Zr/TiO_2 was much better than that of TiO_2 nanotubes under UV irradiation. Nanotube arrays prepared by this method could be reused for more than 20 times and maintained good photocatalytic activities.

Shape-controlled synthesis of gold icosahedra and nanoplates using Pluronic P123 block copolymer and sodium chloride
Won-Ki Lee, Sang-Ho Cha, Ki-Hyun Kim, Byung-Woo Kim and Jong-Chan Lee
Page 3243

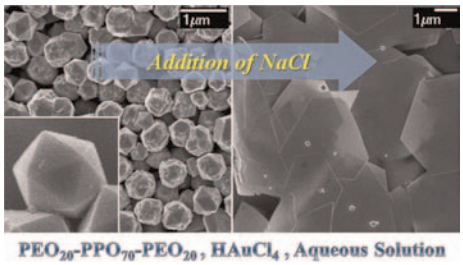

Gold icosahedra were prepared by heating an aqueous solution of Pluronic P123 and $HAuCl_4$. When NaCl was added to this solution, gold nanoplates were produced.

Molten salt synthesis and localized surface plasmon resonance study of vanadium dioxide nanopowders
Fu Wang, Yun Liu and Chun-yan Liu
Page 3249

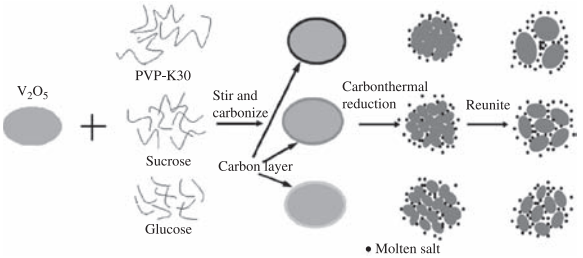

Schematic illustration of the formation mechanism of VO_2(M) nanoparticles in molten salt, particles size can be controlled by choosing organic carbon sources with different chain length.

$K_2Ca_6Si_4O_{15}$—structural and spectroscopical studies on a mixed tetrahedral–octahedral framework
E. Arroyabe, R. Kaindl, D.M. Többens and V. Kahlenberg
Page 3254

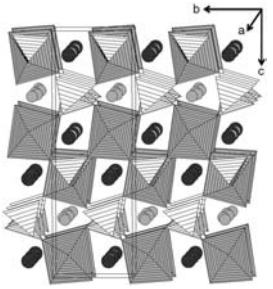

Side view of the whole heteropolyhedral framework in K2Ca6-Si4O15.

Crystal structure and magnetic properties of Li,Cr-containing molybdates $Li_3Cr(MoO_4)_3$, $LiCr(MoO_4)_2$ and $Li_{1.8}Cr_{1.2}(MoO_4)_3$
A. Sarapulova, D. Mikhailova, A. Senyshyn and H. Ehrenberg
Page 3262

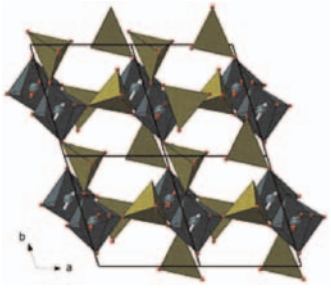

Magnetic structure of $LiCr(MoO_4)_2$. The orientation of the magnetic moments of Cr^{3+} are shown by arrows.

New thallium iodates—Synthesis, characterization, and calculations of $Tl(IO_3)_3$ and $Tl_4(IO_3)_6$, $[Tl_3^+Tl^{3+}(IO_3)_6]$
Jeongho Yeon, Sang-Hwan Kim and P. Shiv Halasyamani
Page 3269

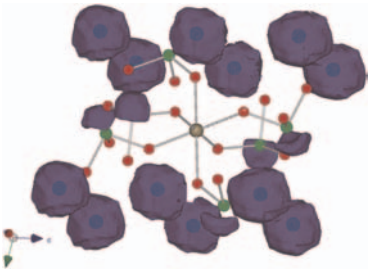

Visualization of the stereo-active lone-pair (purple) through ELFs for $Tl_4(IO_3)_6$. The spherical nature of the ELFs around the Tl^+ cation indicates the lone-pair is inert.

Structural distortions in the spin-gap regime of the quantum antiferromagnet $SrCu_2(BO_3)_2$

C. Vecchini, O. Adamopoulos, L.C. Chapon, A. Lappas, H. Kageyama, Y. Ueda and A. Zorko

Page 3275

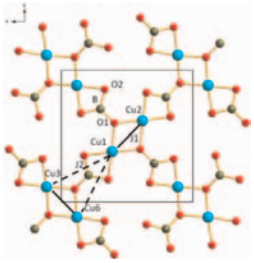

We report the first crystallographic study within the low-temperature spin-gap region of the two-dimensional frustrated antiferromagnet $SrCu_2(BO_3)_2$. Subtle spin-lattice coupling was unveiled in the low-temperature region.

Low temperature molten-salt synthesis of nanocrystalline cubic Sr_2SbMnO_6

Antara Baral and K.B.R. Varma

Page 3282

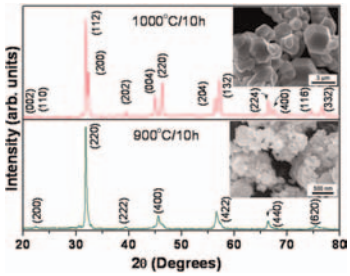

The as synthesized powders of Sr_2SbMnO_6 calcined at 900 °C/10 h yielded a cubic phase (~60 nm sized crystallites). Centrosymmetric tetragonal (*I*4/*mcm*) phase was obtained by increasing the calcination temperature to 1000 °C.

Theoretical investigation of structural stability and lattice vibrations of $U_6Fe_{16}Si_7$ and its interstitial carbide $U_6Fe_{16}Si_7C$

Ping Qian, Qing-Yu Hu and Jiang Shen

Page 3289

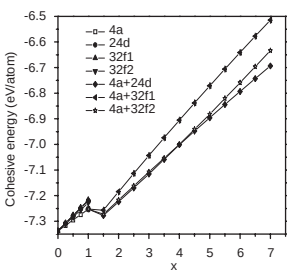

It is seen from the figure that the first silicon atoms to enter the structure fill a high percentage of the 4*a* sites, after which, occupation of the 24*d* sites begin.

Formation of apatite oxynitrides by the reaction between apatite-type oxide ion conductors, $La_{8+x}Sr_{2-x}(Si/Ge)_6O_{26+x/2}$, and ammonia

A. Orera, D. Headspith, D.C. Apperley, M.G. Francesconi and P.R. Slater

Page 3294

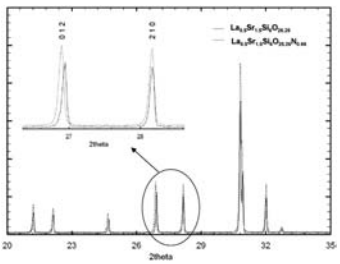

In this paper we show that heating the apatite-type electrolytes $La_{8+x}Sr_{2-x}(Si/Ge)_6O_{26+x/2}$ in NH_3 at high temperatures leads to nitridation of the electrolyte, with the level of nitridation increasing with increasing x.

Electronic structure and photoluminescence properties of Eu^{2+}-activated Ca_2BN_2F

Y.Q. Li, C.M. Fang, Y. Fang, A.C.A. Delsing, G. de With and H.T. Hintzen

Page 3299

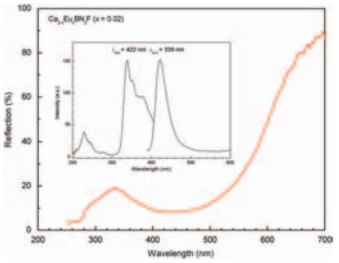

Diffuse reflection spectrum, excitation and emission spectra of Ca_2BN_2F:Eu^{2+}, showing that only the ionic Eu^{2+} center offers deep blue emission at about 422 nm under excitation at 339 nm.

Oxidation behaviour of uranium and neptunium in stabilised zirconia

Marcus Walter, Joseph Somers, Daniel Bouëxière, Piotr Gaczyński and Boris Brendebach

Page 3305

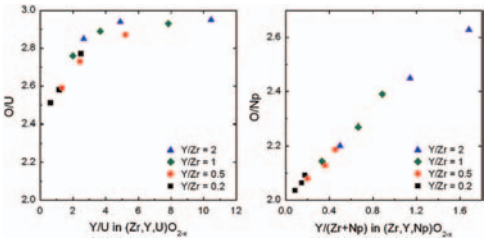

The O/U ratio in oxidised $(Zr,Y,U)O_{2-x}$ depends on the Y/U ratio, whereas O/Np in $(Zr,Y,Np)O_{2-x}$ correlates with the Y/(Zr + Np) ratio. This indicates that both Zr and Np compete for oxygen vacancies, which hinders the Np oxidation at low Y/Zr ratios.

Continued

Structural characterization of C–S–H and C–A–S–H samples—Part I: Long-range order investigated by Rietveld analyses

Guillaume Renaudin, Julie Russias, Fabrice Leroux, Fabien Frizon and Céline Cau-dit-Coumes

Page 3312

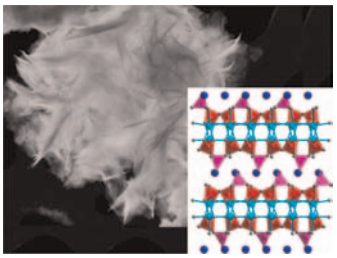

The Tobermorite M model has been successfully used to perform Rietveld analyses on X-ray powder patterns from C–S–H samples. Refinement of the cationic site occupancies explains the evolution from the linear silicate chains to the isolated silicate dimers when increasing the C/S ratio.

Structural characterization of C–S–H and C–A–S–H samples—Part II: Local environment investigated by spectroscopic analyses

Guillaume Renaudin, Julie Russias, Fabrice Leroux, Céline Cau-dit-Coumes and Fabien Frizon

Page 3320

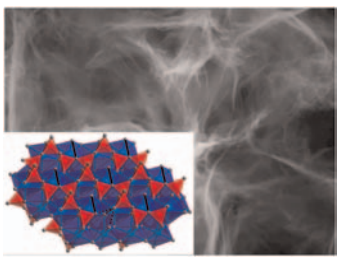

The insertion of aluminum atoms into the C–S–H structure has been investigated by spectroscopic analyses (^{27}Al and ^{1}H MAS NMR and Raman). The previously determined structural continuity, when increasing the C/S ratio from the C–S–H(I) type to the C–S–H(II) type, has been confirmed even in the presence of aluminum.

Intercalation of stable organic radicals into layered inorganic host matrices: Preparation and structural characterization of $Cd_{1-x}PS_3$(*meta*MPYNN)$_{2x}$

Wilhelm L. Hemme, Wataru Fujita, Kunio Awaga and Hellmut Eckert

Page 3330

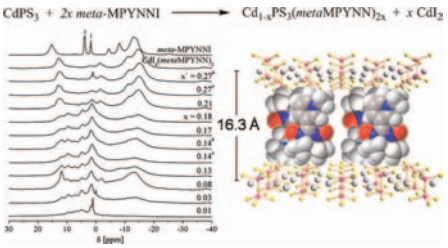

The orientation of a nitroxide radical relative to the $CdPS_3$ layers in the corresponding intercalation compound is inferred from x-ray diffraction and solid state NMR spectroscopy.

Structural and spectroscopic characterization of $Mo_{1-x}W_xO_{3-\delta}$ mixed oxides

S. Morandi, M.C. Paganini, E. Giamello, M. Bini, D. Capsoni, V. Massarotti and G. Ghiotti

Page 3342

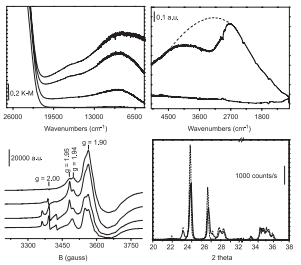

The combined use of different techniques provides new insight into structural, optical and electronic properties of semiconductor $Mo_{1-x}W_xO_{3-\delta}$ mixed oxides.

Preparation and properties of antiperovskite-type nitrides: $InNNi_3$ and $InNCo_3$

W.H. Cao, B. He, C.Z. Liao, L.H. Yang, L.M. Zeng and C. Dong

Page 3353

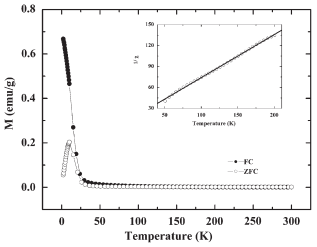

Two ternary nitrides $InNM_3$ (M = Ni, Co) were synthesized by solid–gas reactions of metal powders with NH_3. Both $InNNi_3$ and $InNCo_3$ adopt the antiperovskite crystal structure, and measurements of magnetization indicate that they have spin-glass-like properties.

Evidence of local defects in the oxygen excess apatite $La_{9.67}(SiO_4)_6O_{2.5}$ from high resolution neutron powder diffraction

Stéphanie Guillot, Sophie Beaudet-Savignat, Sébastien Lambert, Rose-Noelle Vannier, Pascal Roussel and Florence Porcher

Page 3358

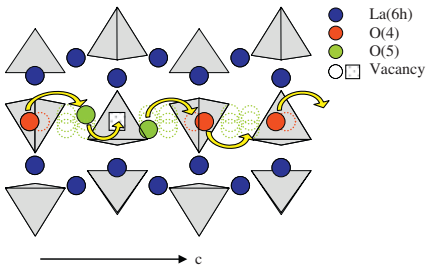

Structural defect position and possible conduction mechanism along the *c*-axis (representation of two adjacent unit-cells).

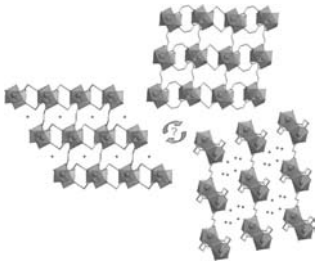

In the field of coordination polymers or MOF's, few studies report on the polymorphs of Ln(III)-succinic acid. Here, we describe the hydrothermal synthesis and structural characterization of two novel yttrium-succinates coordination polymers, respectively 2D and 3D, $Y_2(C_4H_4O_4)_3(H_2O)_4 \cdot 6H_2O$ and $Y_2(C_4H_4O_4)_3(H_2O)_2$.

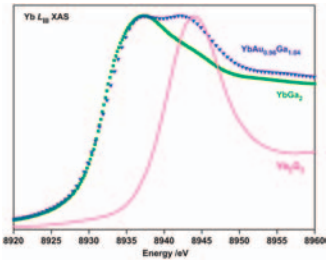

Ordering of the crystal structure in the $YbAu_xGa_{2-x}$ is accompanied by the change of valence of Yb atoms.

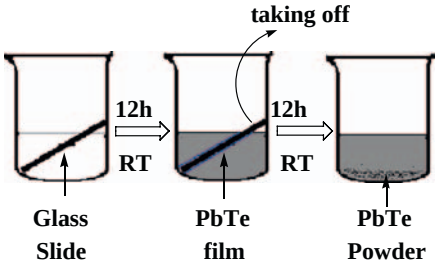

PbTe nanoparticles and films were fabricated at room temperature and ambient pressure in an alkaline aqueous solution by a chemical bath method.

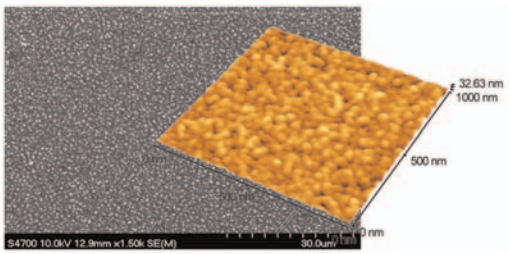

This study has demonstrated that the synthesis of thin layers may be improved and extended if microwave energy is employed during the preparation process. Microwave processing has the potential to reduce the time, cost and energy input for the production of thin layers.

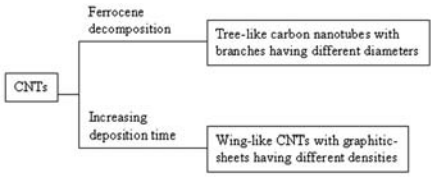

Tree-like carbon nanotubes (CNTs) with branches and the wing-like CNTs with graphitic-sheets were synthesized by using plasma enhanced chemical vapour deposition. The structural dependence of field electron emission property was also investigated.

Tree-like carbon nanotubes (CNTs) with branches and the wing-like CNTs with graphitic-sheets were synthesized by using plasma enhanced chemical vapor deposition. The structural dependence of field electron emission property was also investigated.

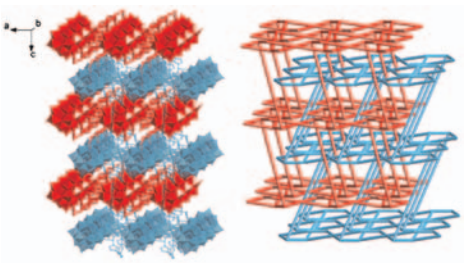

The 3D + 3D structure representation of the first example of interpenetrating framework based on the isopolytungstate.

Continued

Thermo-Raman spectroscopy *in situ* monitoring study of solid-state synthesis of $NiO–Al_2O_3$ nanoparticles and its characterization

Anil Vithal Ghule, Kalyani Ghule, Shin-Hwa Tzing, Tushar H. Punde, Hua Chang and Yong Chien Ling

Page 3406

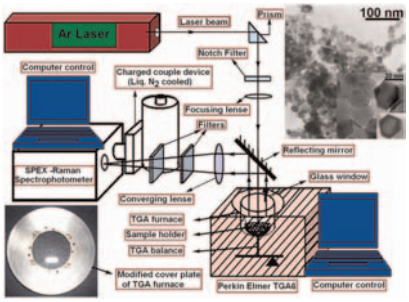

Hyphenation of thermogravimetric analyzer and thermo-Raman spectrophotometer for *in situ* monitoring of solid-state reaction at controlled heating rate and in oxygen atmosphere forming $NiO–Al_2O_3$ catalyst nanoparticles is investigated.

Rapid Communication

On the solid solution of the spinel phase in the system $NiO–Al_2O_3$

Magnus Rotan, Julian Tolchard, Erling Rytter, Mari-Ann Einarsrud and Tor Grande

Page 3412

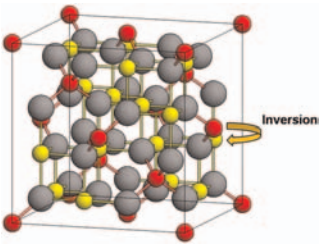

The degree of inversion in the spinel solid solution in the system $NiO–Al_2O_3$ has been investigated. The inversion was little influenced by the Al_2O_3 content and decreases with increasing equilibrated temperature. At room temperature the spinel is close to inverse.

Author inquiries

For inquiries relating to the submission of articles (including electronic submission where available) please visit this journal's homepage at http://www.elsevier.com/locate/jssc. You can track accepted articles at http://www.elsevier.com/trackarticle and set up e-mail alerts to inform you of when an article's status has changed. Also accessible from here is information on copyright, frequently asked questions and more.
Contact details for questions arising after acceptance of an article, especially those relating to proofs, will be provided by the publisher.

Language services. Authors who require information about language editing and copyediting services pre- and post-submission please visit http://www.elsevier.com/locate/languagepolishing or our customer support site at http://epsupport.elsevier.com. Please note Elsevier neither endorses nor takes responsibility for any products, goods or services offered by outside vendors through our services or in any advertising. For more information please refer to our Terms & Conditions http://www.elsevier.com/termsandconditions

For a full and complete Guide for Authors, please go to: http://www.elsevier.com/locate/jssc

Journal of Solid State Chemistry has no page charges.